Back to the Future: Predicting Individual Tau Progression in Alzheimer's Disease

Robin Sandell[1], Justin Torok[1], Kamalini G. Ranasinghe[2], Srikantan S. Nagarajan[1], and Ashish Raj[1*]

[1]Department of Radiology, University of California, San Francisco, CA, USA
[*]Address correspondence to ashish.raj@ucsf.edu

1 Supplemental Figures

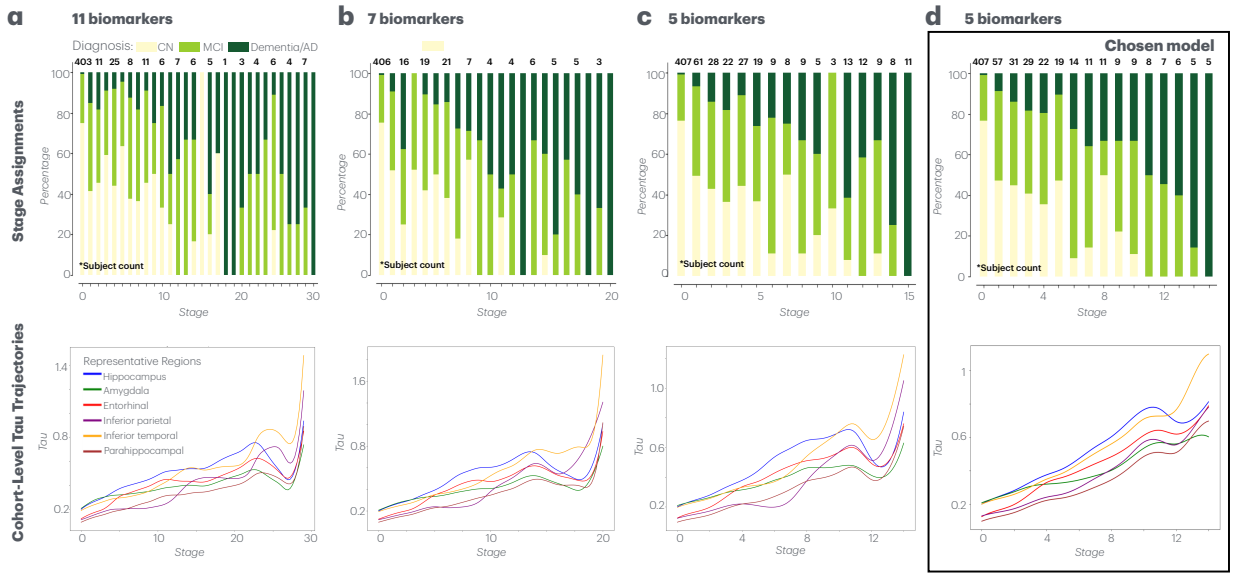

Supplemental Fig 1: Staging module input selection. For each selection of input biomarkers: 1) Histogram of individuals' most likely stage assignment across diagnostic categories and 2) Estimated regional tau distribution across stages in specified regions **a.** Staging module with 11 biomarkers (34 input features) including ADAS11 score, hippocampal volume, and tau in the entorhinal cortex, amygdala, inferior parietal cortex, inferior temporal cortex, hippocampus, parahippocampal gyrus, precuneus, and anterior cingulate. **b.** Staging module with 9 biomarkers (28 input features) including ADAS11 score, hippocampal volume, and tau in the entorhinal cortex, amygdala, hippocampus, precuneus, and anterior cingulate. **c.** Staging module with 5 biomarkers (16 input features) including ADAS11, hippocampal volume, and tau in the entorhinal cortex, amygdala, and inferior parietal cortex.

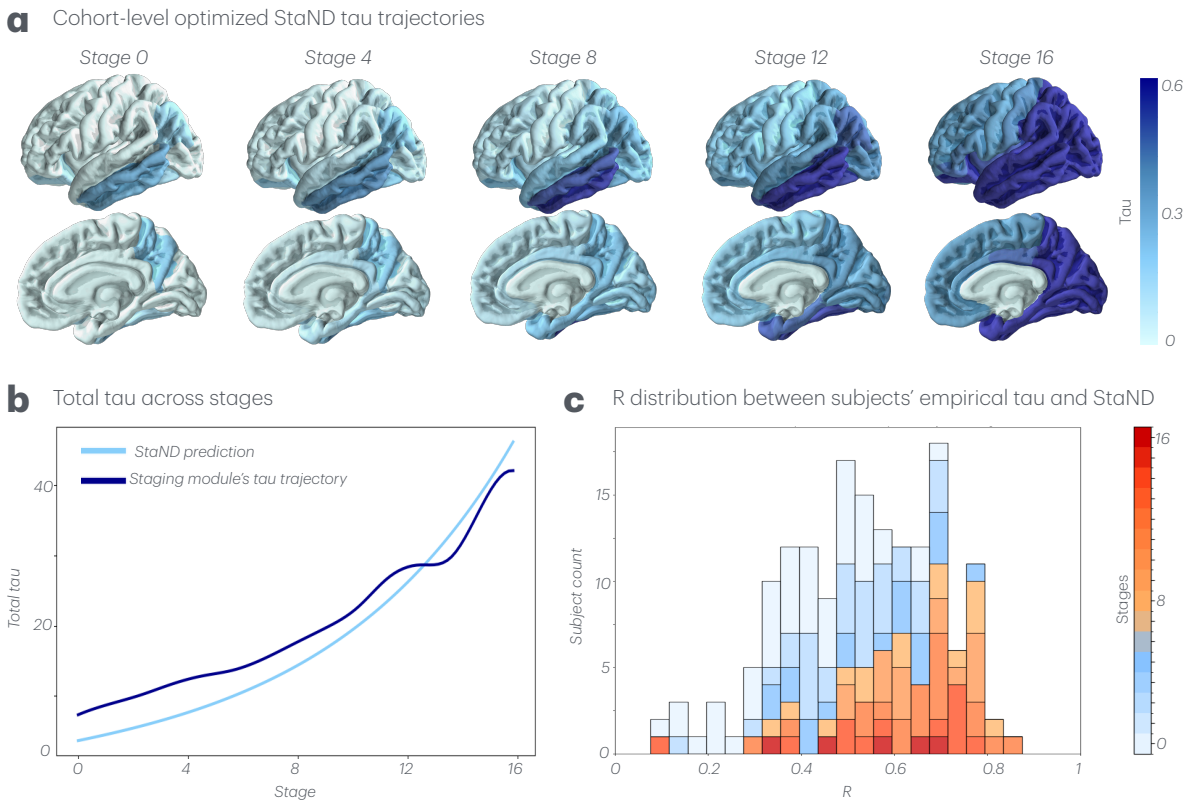

Supplemental Fig 2: Cohort-level inference. **a.** StaND's estimated tau trajectories after iteratively refining cohort-level parameters and tau seed to fit cohort-level tau trajectories from the staging module. **b.**Total tau across stages for both the StaND estimation and staging module-derived cohort-level tau trajectories. **c.** Pearson's R distribution across all subjects between cohort-level StaND and each subject's empirical tau at their assigned stage, colored by subjects' stages.

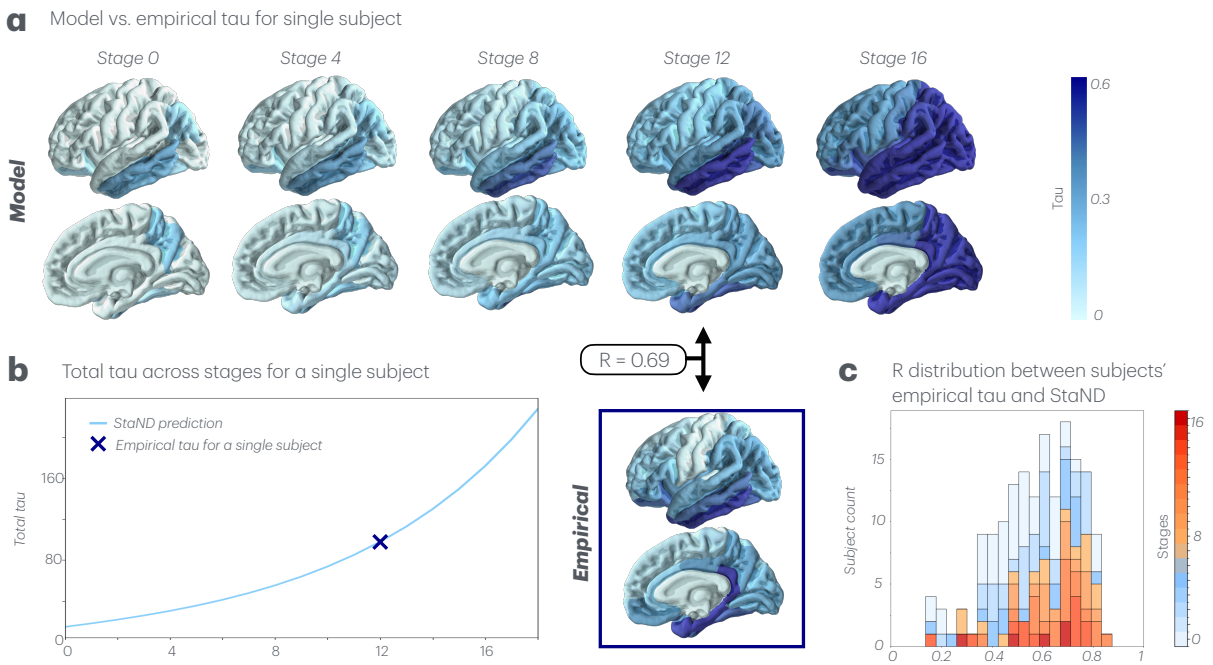

Supplemental Fig 3: StaND with subject-specific parameters and cohort-level seed. a. StaND's estimated tau trajectories and empirical baseline tau for a single subject. **b.** Total tau across stages for the same subject's StaND prediction and empirical tau. **c.** Pearson's R distribution across all subjects between individually-fitted StaND models and empirical tau at each subject's assigned stage, colored by subjects' stage.

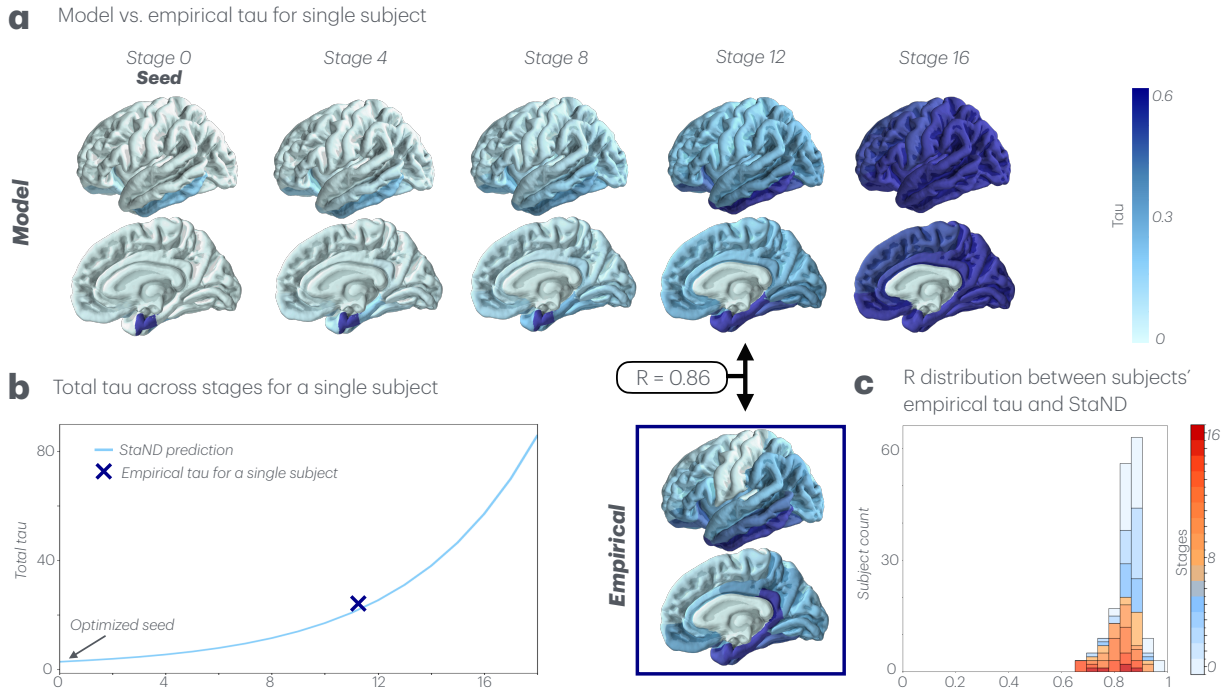

Supplemental Fig 4: StaND with subject-specific seeds and cohort-level parameters. a. StaND's estimated tau trajectories and empirical baseline tau for a single subject. **b.** Total tau across stages for the same subject's StaND prediction and empirical tau. **c.** Pearson's R distribution across all subjects between individually-fitted StaND models and empirical tau at each subject's assigned stage, colored by subjects' stage.

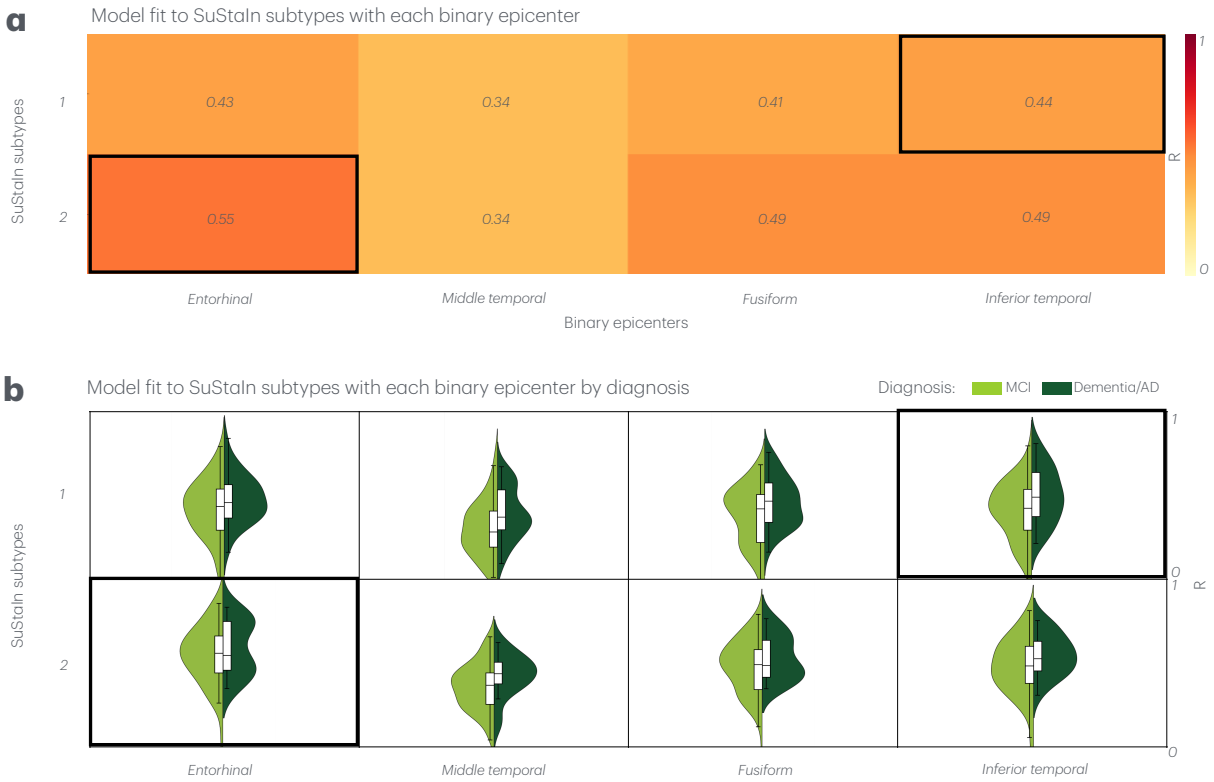

Supplemental Fig 5: Subtype-based benchmark performances. a. Heat map of mean Pearson's R across subjects between model prediction and empirical data for each subtype with each of the four binary epicenters identified by Vogel et al. (2021). Best fitting epicenter for each subtype highlighted. **b**. Violin plots of the distribution of Pearson's R values across subjects for each subtype with each binary epicenter separated by diagnosis. Best fitting epicenter for each subtype again highlighted (and included in the main Figure 4 as our final benchmarks).

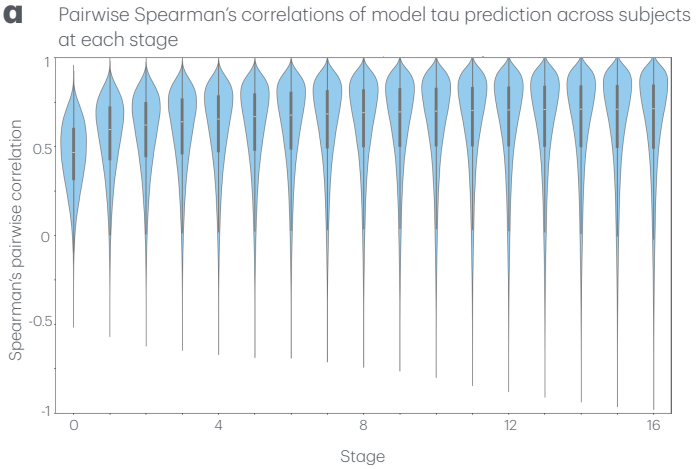

Supplemental Fig 6: a. Distribution of pairwise Spearman's correlations of StaND model predictions across subjects at each stage.

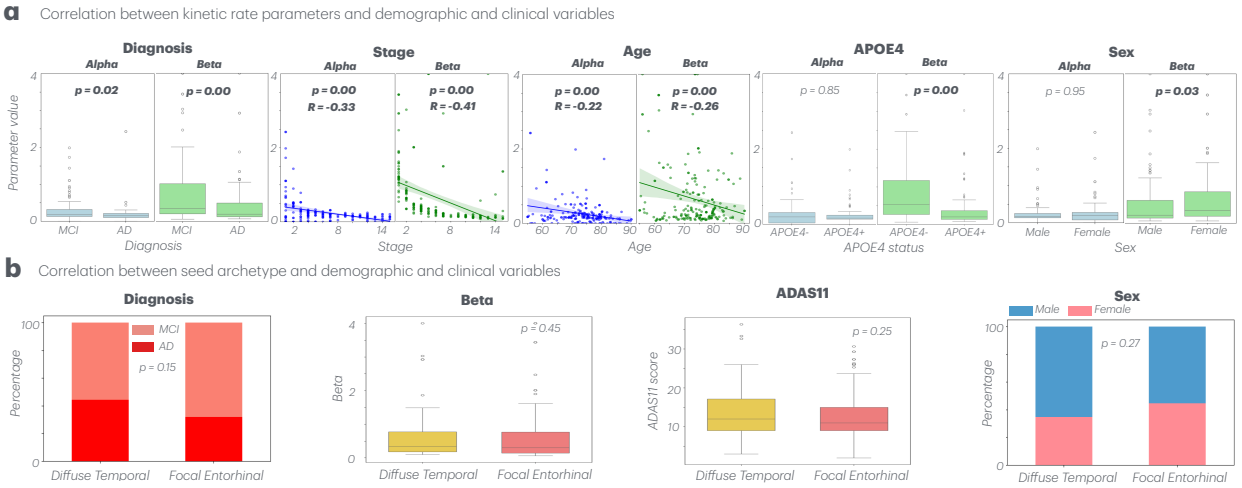

Supplemental Fig 7: Correlations of model output to selected clinical and demographic variables. a. Correlations across subjects between subject-specific kinetic rate parameters – alpha and beta – and a selection of demographic and clinical variables. Categorical variables shown as box plots. Continuous variables shown as scatter plots. Statistically significant relationships in bold. **b.** Demographic, clinical, and model-inferred characteristics of the diffuse temporal and focal entorhinal seed archetypes. Categorical variables shown as percentage distributions. Continuous variables shown as box plots.

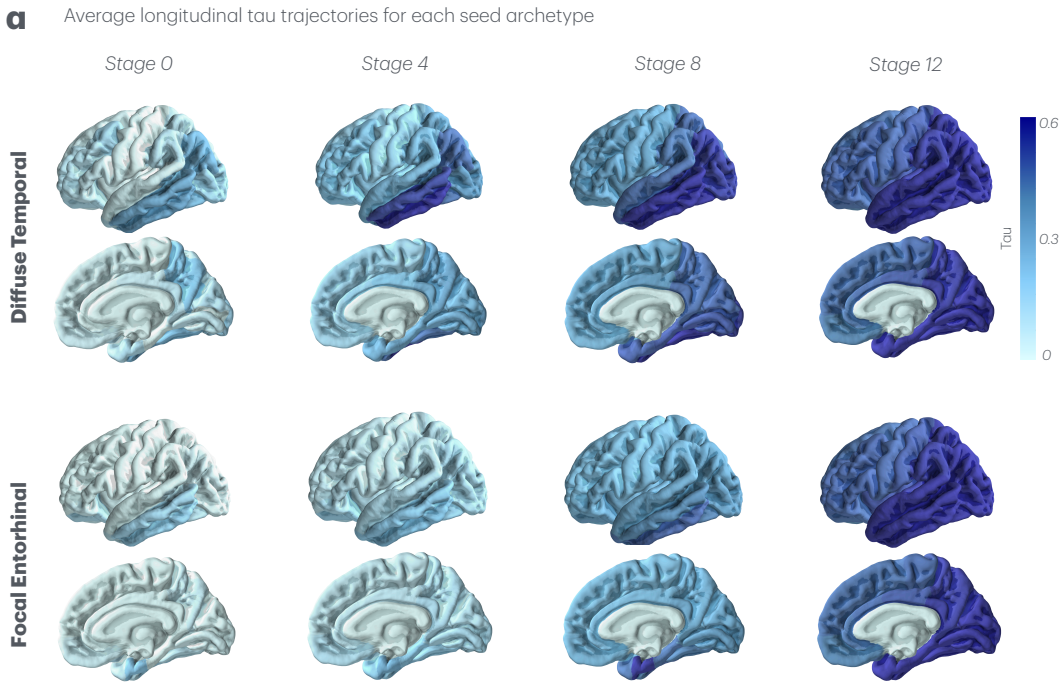

Supplemental Fig 8: a. Average longitudinal tau trajectories of each seed archetype.

2 Supplemental Tables

Seed Region	Mean Value
Right entorhinal	0.317748
Left inferior temporal	0.224544
Right inferior temporal	0.223569
Left middle temporal	0.193884
Left entorhinal	0.186010

Table 1: Highest average tau seed regions across subjects.

3 Supplemental Results

3.1 Justification of selected staging module inputs

We conducted a comprehensive evaluation to determine the optimal biomarker inputs for our staging module. This process involved testing over 25 different configurations with various combinations of AD-relevant biomarkers, including:

- Cognitive assessments: ADAS11, MMSE
- Regional tau-PET measures: hippocampal, entorhinal, inferior parietal, inferior temporal, amygdala, parahippocampal, precuneus, anterior cingulate, and meta-ROI averages
- Volumetric MRI measures: hippocampal, superior frontal, anterior cingulate, posterior cingulate, precuneus, inferior parietal, and inferior temporal volumes

As noted in the main text, the number of input features to the staging module (defined by the number of biomarkers $\times$ the number of severity thresholds fixed at 3) corresponds to complexity and is inherently constrained by the number of samples in our data. To determine the optimal model complexity, we started with 2 biomarker inputs (7 input features) and sequentially added biomarkers up to 11 (34 features). Each was evaluated by their balance of temporal resolution and model robustness. **Supplemental Figure** 1a,b illustrate two higher-complexity iterations of the staging module: one with 11 biomarkers (34 features) and another with 9 biomarkers (28 features). Our analyses revealed that models incorporating more than 5 biomarkers exhibited diminished quality due to insufficient subject representation in advanced stages, compromising effective tau interpolation across these stages. This manifested as non-monotonic increases in interpolated tau values across stages (Supplemental Figure 1a,b).

After establishing that 5 biomarkers provided optimal model performance, we methodically evaluated over 10 different 5-biomarker combinations (Supplemental Figure 1c,d) and evaluated each based on 1) Monotonic increase of tau interpolation across stages, 2) MCMC likelihood (suitable for evaluating fixed-complexity models), and 3) Appropriate staging of diagnostic categories (ie. no control subjects in higher stages or AD subjects in stage 0). As an example, **Supplemental Figure** 1c shows less appropriate staging of diagnostic categories than our chosen selection of biomarkers in 1d, as well as non-monotonic increase of interpolated tau. This rigorous selection process ensured that our final 5-biomarker model achieved the optimal balance between stage resolution and statistical robustness, while maintaining biologically meaningful disease progression patterns.

3.2 Performance comparison across StaND model fitting strategies

Supplemental Figures 2, 3, and 4 illustrate additional StaND optimization strategies we tried: cohort-level inference, subject-specific parameter inference with a cohort-level seed, and subject-specific seed inference with cohort-level parameters. All techniques underperformed relative to our chosen methodology of using subject-specific seeds *and* parameters (mean $R = 0.53, 0.57$, and 0.85 vs. 0.88), indicating that there is heterogeneity of both tau's pattern at disease onset and its accumulation and spread rates across subjects. All details on these methods included in main.

3.3 Top regions across model-inferred subject-specific seeds

The top mean seed regions for StaND with subject-specific seeds are shown in Table 1.

3.4 Benchmarking against subtype-based approaches

For benchmark comparison, we applied the Subtyping and Staging Inference algorithm (SuStaIn), an event-based model used by Vogel et al. (2021), to identify two subtypes within our ADNI3 cohort and employed the inference module to determine the optimal binary tau seed, or "epicenter," for subjects within each subtype. Two subtypes was the ideal number for our dataset because it produced distinct peaks in the model's log likelihood histogram, indicating that the subtypes reflect stable and genuinely differentiable subpopulations. We systematically evaluated each of the four binary tau "epicenters" that Vogel identified as best-fitting their four SuStaIn subtypes, which were derived from a larger and more heterogeneous dataset than ADNI3. Contrary to Vogel's report, we observed no clear one-to-one correspondence between our SuStaIn subtypes and their best-fitting binary epicenters, suggesting substantial seed variability across individual subjects even within statistically defined subtypes (Supplemental Figure 5a). Our proposed StaND method achieves superior empirical fit likely in part because it accounts for this individual heterogeneity rather than assuming within statistical subgroup coherence.

3.5 Non-parametric validation of tau convergence phenomenon using Spearman's correlation

To ensure the robustness of our finding that tau variability across subjects decreases over the course of AD, we performed a Spearman's correlation analysis, which does not assume Gaussian normality of tau distributions. The Spearman correlation of model-predicted tau across subjects over time yielded consistent results with our Pearson correlation findings, confirming that the observed increase in pairwise correlations over time represents a genuine convergence phenomenon rather than an artifact of tau data sparsity or distributional properties (Supplemental Figure 6a). This consistency across both parametric and non-parametric correlation measures strengthens the validity of our core finding that tau patterns as disease progresses.

3.6 Correlating model output to clinical and demographic variables

We additionally correlated model outputs, individual kinetic rate parameters and individual seed patterns, to clinical and demographic variables. Those not shown in main are displayed here. Kinetic rate parameters – tau accumulation rate (α) and tau spread rate (β) – bore statistically significant correlations to diagnosis. Both parameters have a higher mean value for MCI subjects than AD (mean $\alpha = 0.28$ vs. 0.22, KW test: $H = 4.9, p = 0.03$, mean $\beta = 0.74$ vs. 0.48, KW test: $H = 11.5, p = 0.00$; Supplemental Figure 7a). Both parameters decrease with stage ($\alpha : R = -0.33, p = 0.00; \beta : R = -0.41, p = 0.00$) and with age ($\alpha : R = -0.26, p = 0.00; \beta : R = -0.22, p = 0.00$). Tau accumulation rate (α) is higher for APOE- than APOE+ subjects (mean = 0.29 vs. $0.23, p = 0.85$). Spread rate (β) is similarly higher for APOE- subjects (mean = 0.90 vs. $0.44, p = 0.00$). Finally, female subjects had a lower mean α values than male subjects (mean $\alpha = 0.24$ vs. 0.27, KW test: $H = 0.0, p = 0.95$) and a lower mean β value (mean $\beta = 0.55$ vs. 0.73, KW test: $H = 4.71, p = 0.03$) (Supplemental Figure 7a).

The diffuse temporal seed archetype had a higher percentage of AD subjects than the focal entorhinal pattern (44.2% vs. 32.0%, $p = 0.15$), although not with statistical significance as we would expect for a variable that progresses throughout the course of the disease unlike a subject's fixed seed archetype. Diffuse temporal seed subjects have a higher mean spread rate parameter (β) than entorhinal seeding subjects (mean = 0.71 vs. $0.61, p = 0.45$) and higher mean ADAS11 scores (mean = 13.7 vs. $12.5, p = 0.25$), although there is no statistical significance here (Supplemental Figure 7 b). Finally, the diffuse seed group has a higher percentage of male than of female subjects (65.4% vs. 34.6%) and the entorhinal seed group has a higher percentage of female than male (44.7% vs. 55.3%, p = 0.27; Supplemental Figure 7b).

3.7 Distinct longitudinal tau trajectories for each seed archetype

Supplemental Figure 8 illustrates the distinct trajectories of tau for each seed archetype. Tau has distinct origins for each archetype – the temporal cortices and entorhinal cortex – but converges into a common pattern as the disease progresses. These distinct trajectories further substantiate the finding that that tau has heterogeneous origins that converge over time.

4 Supplemental Methods

The following algorithms were used to optimize our Stage-based Network Diffusion model (StaND). All optimization strategies shown.

Algorithm 1 Cohort-level Parameter Optimization

Input: Connectivity matrix C, initial tau vector $\boldsymbol{x}^c(0)$, EBM interpolation data $\boldsymbol{y}$
Output: Optimized model parameters $\boldsymbol{\theta}^c$
// Prepare simulation environment
$U \leftarrow$ Zero or random vector of cell type dimension
$t_{vec} \leftarrow$ Time vector from 0 to 16 stages
// Define error function for the StaND model
function StaND_error($\boldsymbol{\theta}^c$, $\boldsymbol{y}$):
    Initialize Nexis simulation object with:
    - Connectivity matrix C
    - Initial tau vector $\boldsymbol{x}^c(0)$
    - Time vector t_{vec}
    - Additional configuration parameters
    // Unpack optimization parameters
    $\alpha, \beta \leftarrow \boldsymbol{\theta}^c$
    // Simulate StaND model
    $\boldsymbol{x}^c \leftarrow$ Simulate StaND with parameters $\boldsymbol{\theta}^c$
    // Compute error metrics
    Compute MSE and Pearson correlation coefficient between $\boldsymbol{x}^c$ and $\boldsymbol{y}$
    error $\leftarrow \mathcal{E} + 0.5(1 - \mathcal{R})$
    return error
end function
// Define initial parameter guess and bounds
init_guess $\leftarrow$ Initial parameter estimates
bounds $\leftarrow$ Parameter value constraints
// Perform parameter optimization
$\boldsymbol{\theta}^* \leftarrow$ Minimize(StaND_error, init_guess, bounds)
return $\boldsymbol{\theta}^*$

Algorithm 2 Cohort-level Seed Optimization

Input: Connectivity matrix C, fixed parameters $\boldsymbol{\theta}^c = [\alpha, \beta]$, EBM interpolation data $\boldsymbol{y}$, regularization parameter λ
Output: Optimized seed vector $\boldsymbol{x}^c(0)$
// Prepare simulation environment
$U \leftarrow$ Zero vector of dimension nROI $\times$ 1
$t_{vec} \leftarrow$ Time vector from 0 to 10 with 100 points
$w\_dir \leftarrow 0$ // No directionality preference
$volcorrect \leftarrow 1$ // Volume correction flag
// Define error function for seed optimization
function Nexis_MSE($\boldsymbol{x}(0)$, $\boldsymbol{x}$):
    // Set up parameters for simulation
    $parameters \leftarrow [\alpha, \beta, \boldsymbol{x}(0)]$
    // Simulate StaND model with the proposed seed
    $\boldsymbol{x}$ Simulate Nexis with parameters
    // Check if $\boldsymbol{x}$ is constant
    if $\boldsymbol{x}$ is constant **then**
        Add small constant to first element of $\boldsymbol{x}$
    end if
    // Compute error metrics with regularization
    $corr\_coeff \leftarrow$ Pearson correlation between $\boldsymbol{x}$ and $\boldsymbol{y}$
    $error \leftarrow MSE(\boldsymbol{x}, \boldsymbol{y}) + 0.5(1 - corr\_coeff) + \lambda \frac{\|\boldsymbol{x}(0)\|_1}{\sqrt{\sum(\boldsymbol{x}^2(0))}}$
    return error
end function
// Define initial seed guess
$seeding\_locations \leftarrow$ ['ctx-lh-entorhinal', 'ctx-rh-entorhinal']
$seeding\_indices \leftarrow$ Indices of seeding locations in region list
$init\_guess \leftarrow$ Zero vector with 1s at seeding indices
$bounds \leftarrow$ [(0, 3) for each region]
// Perform seed optimization
$\boldsymbol{x}^c(0) \leftarrow$ Minimize(Nexis_MSE, init_guess, bounds, method='L-BFGS-B')
return $\boldsymbol{x}^c(0)$

Algorithm 3 Individual Parameter Optimization

Input: Connectivity matrix C, fixed initial vector $\boldsymbol{x}^c(0)$, individual's empirical tau $\boldsymbol{y}^i$, individual's EBM stage t^i
Output: Optimized individual parameters $\boldsymbol{\theta}^i$
// Prepare simulation environment
$U \leftarrow$ Zero vector of dimension nROI $\times$ 1
$t_{vec} \leftarrow$ Time vector from 0 to 18 with 19 points
$w\_dir \leftarrow 0$ // No directionality preference
$volcorrect \leftarrow 1$ // Volume correction flag
// Define error function for parameter optimization
function Nexis_error($\boldsymbol{\theta}$, $\boldsymbol{y}^i$):
    // Unpack optimization parameters
    $\alpha, \beta \leftarrow \boldsymbol{\theta}$
    // Initialize Nexis model
    Initialize Nexis with connectivity C, initial vector $\boldsymbol{x}^c(0)$, and time vector t_{vec}
    // Simulate StaND model
    $\boldsymbol{x}$ Simulate Nexis with parameters $[\alpha, \beta]$
    // Extract tau values at individual's stage
    $\boldsymbol{x}_{edited} \leftarrow \boldsymbol{x}[:, t^i]$
    // Check if $\boldsymbol{x}$_edited is constant
    if $\boldsymbol{x}_{edited}$ is constant **then**
        Add small constant to first element of $\boldsymbol{x}_{edited}$
    end if
    // Compute error metrics
    $corr\_coeff \leftarrow$ Pearson correlation between $\boldsymbol{x}_{edited}$ and $\boldsymbol{y}^i$
    $error \leftarrow MSE(\boldsymbol{x}_{edited}, \boldsymbol{y}^i) + 0.5(1 - corr\_coeff)$
    return error
end function
// Define initial parameter guess and bounds
$init\_guess \leftarrow$ Initial parameter estimates
$bounds \leftarrow$ Parameter value constraints
// Perform parameter optimization
$\boldsymbol{\theta}^i \leftarrow$ Minimize(Nexis_error, init_guess, bounds, method='Powell')
return $\boldsymbol{\theta}^i$

Algorithm 4 Individual Seed Optimization

Input: Connectivity matrix C, fixed parameters $\boldsymbol{\theta}^c = [\alpha, \beta]$, individual's empirical tau $\boldsymbol{y}^i$, individual's EBM stage t^i, regularization parameter λ
Output: Optimized individual seed vector $\boldsymbol{x}^i(0)$
// Prepare simulation environment
$U \leftarrow$ Zero vector of dimension nROI $\times$ 1
$t_{vec} \leftarrow$ Time vector from 0 to 18 with 19 points
$w\_dir \leftarrow 0$ // No directionality preference
$volcorrect \leftarrow 1$ // Volume correction flag
// Define error function for individual seed optimization
function Nexis_MSE($\boldsymbol{x}(0)$, $\boldsymbol{y}^i$, t^i):
    // Set up parameters for simulation
    $parameters \leftarrow [\alpha, \beta, \boldsymbol{x}(0)]$
    // Simulate StaND model with the proposed seed
    $\boldsymbol{x}_{edited}$ Simulate Nexis with parameters
    // Extract tau values at individual's stage
    $\boldsymbol{x}_{edited} \leftarrow Y[:, t^i]$
    // Check for constant arrays
    if $\boldsymbol{y}^i$ is constant **or** $\boldsymbol{x}_{edited}$ is constant **then**
        return $1e10$ // Very high error
    end if
    // Compute error metrics with regularization
    $corr\_coeff \leftarrow$ Pearson correlation between $\boldsymbol{x}_{edited}$ and $\boldsymbol{y}^i$
    $error \leftarrow MSE(\boldsymbol{x}_{edited}, \boldsymbol{y}^i) + 0.5(1 - corr\_coeff) + \lambda \frac{\|\boldsymbol{x}_0\|_1}{\sqrt{\sum(\boldsymbol{x}^2(0))}}$
    return error
end function
// Define initial seed guess
$seeding\_locations \leftarrow$ ['ctx-lh-entorhinal', 'ctx-rh-entorhinal']
$seeding\_indices \leftarrow$ Indices of seeding locations in region list
$init\_guess \leftarrow$ Zero vector with 1s at seeding indices
$bounds \leftarrow$ [(0, 3) for each region]
// Perform seed optimization
$\boldsymbol{x}^i(0) \leftarrow$ Minimize(Nexis_MSE, init_guess, bounds, method='L-BFGS-B')
return $\boldsymbol{x}^i(0)$